

Topological spin phases of trapped Rydberg excitons in Cu₂O

A.N. Poddubny and M.M. Glazov
*Ioffe Institute, St. Petersburg 194021, Russia**
 (Dated: March 29, 2019)

We study theoretically Rydberg excitons in one-dimensional chains of traps in Cu₂O coupled via the van der Waals interaction. The triplet of optically active p -shell states acts as an effective spin-1 and the interactions between the excitons are strongly spin-dependent. We predict that the system has the topological Haldane phase with the diluted antiferromagnetic order, long-range string correlations, and finite excitation gap. We also analyze the effect of the trap geometry and interactions anisotropy on the Rydberg exciton spin states and demonstrate that a rich spin phase diagram can be realized showing high tunability of the Rydberg exciton platform.

Introduction. Rydberg states of matter attract high interest nowadays. Strongly excited atoms are macroscopic quantum objects highly susceptible to external fields that serve for bench-top studies of quantum effects at a large scale [1]. Enhanced polarizability of Rydberg atoms results in efficient interactions making them a platform of choice for quantum simulations [2].

Exciton, the Coulomb interaction correlated electron-hole pair, emerges in semiconductors when an electron is promoted optically from the filled valence to an empty conduction band. It is a direct analogue of the hydrogen-like atom [3]. Perfectness of the natural cuprous oxide crystals has not only made it possible to discover large-radius excitons in semiconductors [4] but has lead also to a recent breakthrough: demonstration of stable highly-excited excitonic Rydberg states with principal quantum number n up to 25 [5]. By contrast to Rydberg atoms excitons exist in the crystalline environment, which manifests itself not only in quantitative differences of the binding energy and exciton radii, but also in different selection rules for optical transitions [6–8] making p -shell excitons with the orbital angular momentum 1 active in single-photon processes, unusual fine structure of the energy spectrum [9], as well as broken symmetries [10, 11]. All this provides flexibility to control the excitonic states by light.

Even more rich consequences of the non-zero orbital angular momentum are expected in exciton-exciton interactions in cuprous oxide [12], which, just like for atoms, are of paramount importance for Rydberg excitons physics [5]. By now, the interactions are scarcely studied, however, according to the recent theoretical predictions [12], the coupling between the excitonic states crucially depends on the mutual orientations of their angular momenta.

Similarly to atomic physics, the interaction effects are expected to be strongest in ensembles of localized Rydberg excitons. Here we demonstrate that already in a one-dimensional chain of trapped Rydberg excitons in Cu₂O the ground state corresponds to a topologically non-trivial spin order — the Haldane phase [13] — with diluted antiferromagnetic order and a gapped spectrum of elementary excitations. Such a topological phase is

inherent to integer spin, in particular spin-1, chains with antiferromagnetic coupling. The hallmarks of the Haldane phase are the non-trivial edge states behaving akin spin-1/2 fermions as well as the presence of the hidden long-range “string” order despite the apparent lack of distant spin-spin correlations [14]. Despite numerous theoretical proposals [15], so far the Haldane phase has been only probed by the neutron scattering [16] or heat conductivity measurements [17, 18] in anisotropic magnetic materials.

Thus, the Rydberg excitons provide a highly desirable table-top solid state platform with direct optical access to individual excitons for both fundamental studies of hidden symmetries and topological orders and prospective quantum simulations [15, 19–22].

Chain of Rydberg excitons. We consider Rydberg excitons confined in a one-dimensional (1D) periodic array of traps, see Fig. 1. The traps for excitons could be created either optically utilizing the ac Stark shift of excitons in the structured light waves, similar to the optical lattices of cold atoms [23] or in tailored semiconductor environment where the band gap energy can be controlled by applying the strain or external electrostatic potential [24]. It is assumed that each trap is occupied by a single exciton, that is in a p -shell state with the angular momentum of the envelope function being equal to 1. For simplicity, we neglect here exciton internal spin degrees of freedom, i.e., the spins of electrons and holes, and the spin-orbit interaction. We introduce the pseudovector angular momentum operator $\mathbf{S}_j = (S_j^x, S_j^y, S_j^z)$ for j th trap. Hereafter, we use the term spin to denote \mathbf{S}_j for brevity, z is the chain axis. We assume that the traps are sufficiently well separated, thus the excitons in

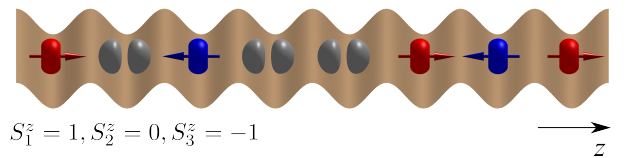


FIG. 1. Schematics of the diluted antiferromagnetic state formed from p -shell Rydberg excitons in an array of traps

neighboring traps are coupled to each other by the van der Waals interaction only. Owing to strong, R^{-6} , decay of the potential with the distance between the traps R , it is sufficient to consider the nearest neighbor approximation. The Hamiltonian of the chain has the form $\mathcal{H} = \sum_{j=1}^{N-1} \mathcal{H}_{\text{bond}}(\mathbf{S}_j, \mathbf{S}_{j+1})$, where N is the number of traps equal to the number of excitons in the system, $\mathcal{H}_{\text{bond}}$ is the neighbors coupling Hamiltonian. The system has a rotational symmetry around the z axis. Thus, $\mathcal{H}_{\text{bond}}$ is characterized by 7 real constants [25] c_0, \dots, c_6 and can be presented as

$$\begin{aligned} \mathcal{H}_{\text{bond}}(\mathbf{S}_1, \mathbf{S}_2) = & c_0 + c_1 S_1^z S_2^z + c_2 (S_1^x S_2^x + S_1^y S_2^y) \quad (1) \\ & + c_3 (S_1^z S_2^z)^2 + c_4 (S_1^x S_2^x + S_1^y S_2^y)^2 \\ & + c_5 [S_1^z S_2^z (S_1^x S_2^x + S_1^y S_2^y) + \text{H.c.}] \\ & + c_6 (S_1^x S_2^y - S_1^y S_2^x)^2. \end{aligned}$$

The microscopic calculation in Ref. [12] confirms that all 7 parameters are significant. Specifically, for the exciton with principal quantum numbers $n = 12 \dots 25$ one has [12]

$$\begin{aligned} c_0 = -5.58\mathcal{E}, c_1 = 9.53\mathcal{E}, c_2 = -8.97\mathcal{E}, \\ c_3 = 1.27\mathcal{E}, c_4 = 6.59\mathcal{E}, c_5 = -3.18\mathcal{E}, c_6 = 5.04\mathcal{E}. \quad (2) \end{aligned}$$

where the common factor \mathcal{E} is $n^{15} \times 10 / (2\pi)$ mHz $\times \mu\text{m}^6 / R^6$. It is assumed that the trap size d exceeds by far the exciton size but is much smaller than the distance between the traps R . In this situation the interaction Hamiltonian is independent of the trap size and geometry in the leading order in $d/R \ll 1$. The Hamiltonian is invariant to the change of parameters $c_2 \rightarrow -c_2, c_5 \rightarrow -c_5$ which corresponds to reflection $z \rightarrow -z$ for every second spin. Importantly, the spin-spin coupling is mostly antiferromagnetic ($c_1 > 0$) and strongly anisotropic.

Since the Rydberg blockade prevents two particles from being close to each other [1, 2, 5], in what follows we neglect the exciton tunneling between the traps. The interplay of the interactions and tunneling can enrich the spin phases in bosonic systems [26]. The trap, however, can effect angular momentum state of the exciton giving rise to the anisotropic single particle contributions [27]. We first disregard the anisotropy and discuss its effect in the end of the paper.

Ground and excited state energies. The chain Hamiltonian can not be diagonalized analytically for $N > 3$. Instead, we first solved numerically for the lowest energy states in small finite chains ($N \leq 14$) with the periodic boundary conditions [28]. The results of calculation are shown in Fig. 2. The ground state energy, shown in the inset, quickly converges to the value of $E_0 \approx -3.51N\mathcal{E}$. The ground state is non-degenerate for periodic boundary conditions and has the total spin $\sum_j S_j^z = 0$. The system is gapped, with the excitation gap slowly decreasing with the size. The lowest excited state has zero total spin projection and the excitation energy $E_g \gtrsim 1.1\mathcal{E}$ (red

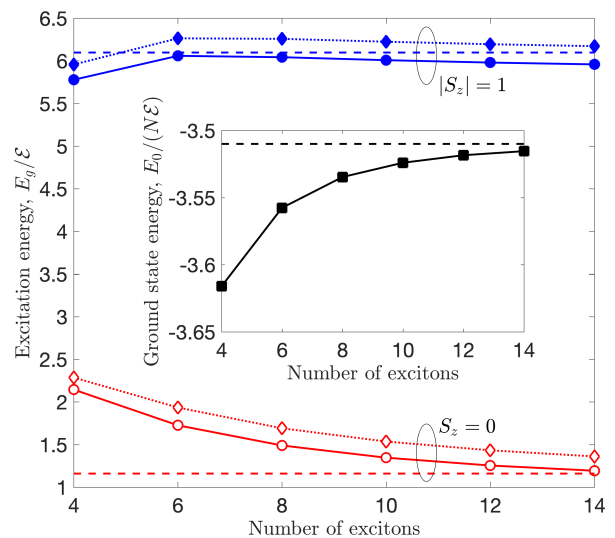


FIG. 2. Ground and excited state energies in spin chains of different lengths with the periodic boundary conditions. Open symbols correspond to the lowest excited state with the total spin projection $\sum S_j^z = 0$, filled symbols correspond to the double-degenerate states with $\sum S_j^z = \pm 1$. Squares indicate results of direct numerical calculation, diamonds correspond to the energies of the variational states Eqs. (3) and (4) with $k = \pi$ and 0, respectively. Dashed lines are the variational results obtained for the infinite system. Inset shows the ground state energy per bond, $E_0/(N\mathcal{E})$, for the finite chain (symbols) and the infinite chain (dashed line).

open symbols in Fig. 2). The states with $\sum_j S_j^z = \pm 1$ have significantly larger excitation energies $E'_g \gtrsim 6\mathcal{E}$ (blue filled symbols). In order to reveal the structure of the excited states we have compared the results of exact diagonalization with those obtained from the single-magnon variational approach [29, 30]. Namely, we used the trial wavefunction

$$\psi_k \propto \frac{1}{\sqrt{N}} \sum_{j=1}^N e^{ikj} S_j^z \psi_0, \quad (3)$$

for the first excited state, where ψ_0 is the numerically calculated ground state, and the wave vector has been set to $k = \pi$ [27]. The variational energy is close to the exact one, which indicates that the excited state is well described by the ansatz Eq. (3). The large overlap (about 0.99) between Eq. (3) and the lowest excited state has been also confirmed numerically. The lowest excited states with the ± 1 total spin projection being degenerate due to the time-reversal symmetry were sought in the form

$$\psi_k \propto \frac{1}{\sqrt{N}} \sum_{j=1}^N e^{ikj} [\mu_1 S_j^z + \mu_2 S_j^z (S_j^x \pm i S_j^y)] \psi_0, \quad (4)$$

with $k = 0$ [27] and $\mu_{1,2}$ being the variational coefficients. The energy of this trial state is close to the exact numerical result as well, cf. blue circles and diamonds in Fig. 2.

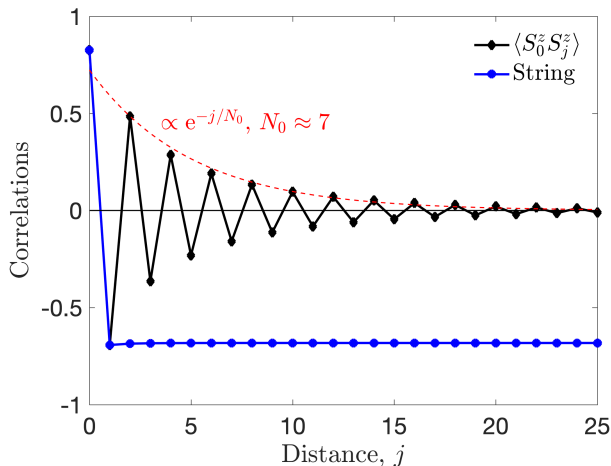


FIG. 3. Spin-spin correlator $(-1)^j C_{\text{Néel}}(j)$ and string correlator for ground state of the infinite chain of Rydberg excitons, Eqs. (6) and (7).

In addition to the exact diagonalization of small finite chains we have also employed the infinite time-evolving block decimation (iTEBD) approach [31–33]. The advantage of this numerical technique is that it is capable to directly address infinite chains. It is based on the representation of the ground state ψ_0 in the matrix-product form [34]

$$\psi_{i_1 i_2 i_3 \dots} \propto M_{\alpha_1 \alpha_2}^{i_1} M_{\alpha_2 \alpha_3}^{i_2} M_{\alpha_3 \alpha_4}^{i_3} \dots, \quad (5)$$

where M is a certain 3-rd rank tensor, indices $i_j = 0, +1, -1$ label the projections of the spin j and $\alpha_j = 1 \dots \chi$ are auxiliary indices. If the spins were independent, one could use $\chi = 1$, so that the α indices are suppressed, $M_{\alpha_j \alpha_{j+1}}^i \rightarrow M^i$ and the state Eq. (5) would reduce to a simple product state. For $\chi > 1$ the state Eq. (5) can describe quantum entanglement (i.e., correlations) between the spins. The iTEBD approach enables high-accuracy description of arbitrary gapped noncritical 1D systems with local Hamiltonians [34, 35] at relatively low computational cost. In our case the convergence of energy better than 1% has been already reached for the rank $\chi \lesssim 20$.

The iTEBD results for the infinite system are shown in Fig. 2 by dashed horizontal lines. The energies of both ground and excited states well agree with the corresponding results for the finite chains. The excited state energies in the infinite system were estimated using the same variational approximation Eqs. (3) and (4) with ψ_0 being now the ground state found from iTEBD. We have also calculated the dispersion of excitations $E_g(k)$ in the single magnon approximation [27]. In agreement with the analysis of the finite system, the spin-0 magnon branch is indeed gapped with the minimum at the edge of the Brillouin zone, $k = \pi$, while the magnons with ± 1 spin projection have the minimum energy at $k = 0$.

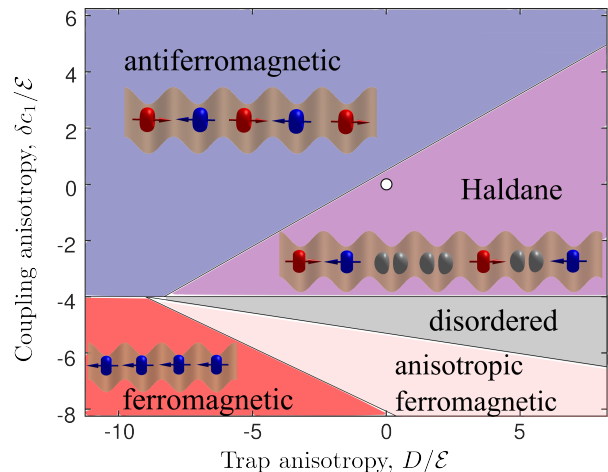


FIG. 4. Phase diagram of the ground state depending on the trap anisotropy and the spin-spin coupling anisotropy. Insets illustrate the typical spin configurations. White circle indicates the parameters of Ref. [12] ($D = \delta c_1 = 0$).

Spin structure of the ground state. Now we proceed to the analysis of the spin-spin correlations in the ground state. The calculation has been performed for the infinite chain using the iTEBD technique. The results are shown in Fig. 3. We start with the analysis of the pair spin-spin correlations depending on the spin-spin distance j . The calculation demonstrates the presence of short-range antiferromagnetic Néel order,

$$C_{\text{Néel}}(j) \equiv (-1)^j \langle S_0^z S_j^z \rangle, \quad (6)$$

At large distances the spin correlations Eq. (6) vanish, as illustrated by the red dashed curve in Fig. 3 showing the exponential decay with the correlation length ≈ 7 . Hence, based only on the analysis of local spin-spin correlations one could conclude that the considered spin phase has no long-range order. However, this is not the case. Our main result is that the infinite chains of Rydberg excitons do possess a long-range string order, characterized by the non-vanishing correlator [14]

$$C_{\text{string}}(j) = \langle S_0^z e^{i\pi(S_1^z + S_2^z + \dots + S_{j-1}^z)} S_j^z \rangle, \quad (7)$$

blue circles in Fig. 3. The presence of the non-local order parameter $C_{\text{string}}(j)$ can be interpreted as a result of spontaneous breaking of a certain $\mathbb{Z}_2 \times \mathbb{Z}_2$ symmetry, hidden in the system [36]. Such string order in the absence of Néel order has been first revealed in the Affleck-Kennedy-Lieb-Tasaki (AKLT) model with $\mathcal{H}_{\text{bond}} = \mathbf{S}_1 \cdot \mathbf{S}_2 + (\mathbf{S}_1 \cdot \mathbf{S}_2)^2/3$ [37, 38]. The AKLT model is exactly solvable by the matrix product state Eq. (5) with certain rank-2 matrices [36]. Similar ansatz has allowed us to obtain analytically the ground state energy with $E_0 = -3.49N\mathcal{E}$ [27], which is very close to the numerically obtained value of $E_0 = -3.51N\mathcal{E}$ shown in the inset of Fig. 2. The simultaneous presence of the

string order and the absence of the Néel order, along with the presence of the non-degenerate gapped ground state are the clear fingerprints of the Haldane phase of spin-1 excitons [13, 39]. Physically, this indicates so-called diluted antiferromagnetism where the wavefunction of the ground state ψ_0 can be represented as a superposition of basic functions in the form

$$|\dots, 0\dots, 0, 1, -1, 0, \dots, 1, -1, 1, 0\dots\rangle,$$

where the significant part of excitons is in the $S^z = 0$ state, and the spins $S^z = \pm 1$ can occur only in pairs, i.e., $+1, -1$ or $-1, +1$, while the pairs $+1, +1$ or $-1, -1$ are forbidden. Thus, the string correlator singles out “diluted antiferromagnetic order”, where neighboring spins are always opposite with the possible arbitrary number of zeroes in between. The fact that the pair $+1, -1$ or $-1, +1$ can occur at any arbitrary place of the chain is related to the formation of the topological Haldane phase in our system. Such diluted antiferromagnetic state is schematically illustrated in Fig. 1.

The shooting gun evidence for the Haldane phase is the presence of edge states in a finite chain with open boundary conditions behaving as spin-1/2 fermions [14, 20]. Our numerical calculations for $N \leq 14$ exciton chains have indeed confirmed that, in the case of open boundary conditions, the ground state corresponds to 4 closely lying levels corresponding to the combinations of edge spins-1/2 slightly split due to the finite chain size [27].

Phase diagram. The Haldane phase is a robust generic feature of 1D spin-1 chains with antiferromagnetic nearest-neighbor interaction. For instance, it is known to exist in isotropic bilinear-biquadratic spin chains with $\mathcal{H}_{\text{bond}} = -\cos\theta \mathbf{S}_1 \cdot \mathbf{S}_2 + \sin\theta (\mathbf{S}_1 \cdot \mathbf{S}_2)^2$ in a wide range of angles around $\theta = \pi$, including the spin-1 anisotropic Heisenberg model [40]. In order to demonstrate, that the formation of the Haldane phase for the Rydberg excitons is not a coincidence, we have analyzed the structure of the ground state depending on the anisotropy of the trap shape and on the sign of the coupling, either ferromagnetic or antiferromagnetic. The trap anisotropy has been described by adding the single particle terms $\mathcal{H}_1 = D \sum_j [(S_j^z)^2 - 2/3]$ to the Hamiltonian [27]. The coupling anisotropy was described by additional term $\delta c_1 S_1^z S_2^z$ in the bond Hamiltonian Eq. (1). The structure of the ground state was determined from comparison of the spin-spin and string correlations at large distances. The results of this analysis are summarized in Fig. 4, and the correlation functions are given in the Supplementary Materials [27].

We start the discussion of the phase diagram Fig. 4 with the role of the coupling term $\delta c_1 S_1^z S_2^z$. Clearly, for large positive δc_1 the spin-spin interaction becomes antiferromagnetic, $\langle S_1^z S_2^z \rangle = -1$, while for negative δc_1 the system is driven in the ferromagnetic phase with $\langle S_1^z S_2^z \rangle = 1$. The anisotropic ferromagnetic order, indicated by pink area in Fig. 4, is characterized by the

long-range spin-spin correlations with $\langle S_1^z S_2^z \rangle < 1$. The Haldane phase is realized in the antiferromagnetic regime in the wide range of the trap anisotropy parameter D provided that it is not large negative. The impact of the anisotropy has also a transparent interpretation: Large positive values of D favor $S^z = 0$ ground state first facilitating the formation of the diluted antiferromagnetic state and, ultimately, the non-magnetic state with $S_j^z \equiv 0$ at each site. Similarly to the spin-1 Heisenberg model even slight anisotropy $D < 0$ switches the system into the antiferromagnetic state [41]. Large negative values of D push down $S^z = \pm 1$ states rendering the exciton chain to the set of 1/2-pseudospins and suppressing the Haldane phase.

Acknowledgements. We are grateful to M. Aßmann, M. Bayer, T. Pohl, M.A. Semina, and V. Walther for fruitful discussions.

-
- * poddubny@coherent.ioffe.ru; glazov@coherent.ioffe.ru
- [1] T. Gallagher, *Rydberg Atoms*, Cambridge Monographs on Atomic Physics (Cambridge University Press, 2005).
 - [2] M. Saffman, T. G. Walker, and K. Mølmer, “Quantum information with Rydberg atoms,” *Rev. Mod. Phys.* **82**, 2313–2363 (2010).
 - [3] E. I. Rashba and M. D. Sturge, eds., *Excitons* (North-Holland Publishing Company, 1982).
 - [4] E. F. Gross and N. A. Karjzew, “Light absorption by cuprous oxide crystal in infrared and visible part of the spectrum,” *Dokl. Akad. Nauk SSSR* **84**, 471 (1952).
 - [5] T. Kazimierzczuk, D. Fröhlich, S. Scheel, H. Stolz, and M. Bayer, “Giant Rydberg excitons in the copper oxide Cu₂O,” *Nature* **514**, 343 (2014).
 - [6] S. Zielińska-Raczyńska, G. Czaikowski, and D. Ziemkiewicz, “Optical properties of Rydberg excitons and polaritons,” *Phys. Rev. B* **93**, 075206 (2016).
 - [7] J. Heckötter, M. Freitag, D. Fröhlich, M. Aßmann, M. Bayer, M. A. Semina, and M. M. Glazov, “Scaling laws of Rydberg excitons,” *Phys. Rev. B* **96**, 125142 (2017).
 - [8] M. A. Semina, “Fine structure of Rydberg excitons in cuprous oxide,” *Physics of the Solid State* **60**, 1527–1536 (2018).
 - [9] J. Thewes, J. Heckötter, T. Kazimierzczuk, M. Aßmann, D. Fröhlich, M. Bayer, M. A. Semina, and M. M. Glazov, “Observation of high angular momentum excitons in cuprous oxide,” *Phys. Rev. Lett.* **115**, 027402 (2015).
 - [10] M. Aßmann, J. Thewes, D. Fröhlich, and M. Bayer, “Quantum chaos and breaking of all anti-unitary symmetries in Rydberg excitons,” *Nature Materials* **15**, 741–745 (2016).
 - [11] F. Schweiner, J. Main, and G. Wunner, “Magnetoexcitons break antiunitary symmetries,” *Phys. Rev. Lett.* **118**, 046401 (2017).
 - [12] V. Walther, S. O. Krüger, S. Scheel, and T. Pohl, “Interactions between Rydberg excitons in Cu₂O,” *Phys. Rev. B* **98**, 165201 (2018).

- [13] F. D. M. Haldane, “Nonlinear field theory of large-spin Heisenberg antiferromagnets: Semiclassically quantized solitons of the one-dimensional easy-axis Néel state,” *Phys. Rev. Lett.* **50**, 1153–1156 (1983).
- [14] M. den Nijs and K. Rommelse, “Preroughening transitions in crystal surfaces and valence-bond phases in quantum spin chains,” *Phys. Rev. B* **40**, 4709–4734 (1989).
- [15] J. Xu, Q. Gu, and E. J. Mueller, “Realizing the Haldane phase with bosons in optical lattices,” *Phys. Rev. Lett.* **120**, 085301 (2018).
- [16] W. Lu, J. Tuchendler, M. von Ortenberg, and J. P. Renard, “Direct observation of the Haldane gap in NENP by far-infrared spectroscopy in high magnetic fields,” *Phys. Rev. Lett.* **67**, 3716–3719 (1991).
- [17] A. V. Sologubenko, T. Lorenz, J. A. Mydosh, A. Rosch, K. C. Shortsleeves, and M. M. Turnbull, “Field-dependent thermal transport in the Haldane chain compound NENP,” *Phys. Rev. Lett.* **100**, 137202 (2008).
- [18] T. Kawamata, Y. Miyajima, N. Takahashi, T. Noji, and Y. Koike, “Large thermal conductivity due to spins in the Haldane gap system Y2BaNiO5,” *Journal of Magnetism and Magnetic Materials* **310**, 1212 – 1214 (2007).
- [19] A. Imambekov, M. Lukin, and E. Demler, “Spin-exchange interactions of spin-one bosons in optical lattices: Singlet, nematic, and dimerized phases,” *Phys. Rev. A* **68**, 063602 (2003).
- [20] F. Pollmann, E. Berg, A. M. Turner, and M. Oshikawa, “Symmetry protection of topological phases in one-dimensional quantum spin systems,” *Phys. Rev. B* **85**, 075125 (2012).
- [21] C. Nayak, S. H. Simon, A. Stern, M. Freedman, and S. Das Sarma, “Non-abelian anyons and topological quantum computation,” *Rev. Mod. Phys.* **80**, 1083–1159 (2008).
- [22] C.-K. Chiu, J. C. Y. Teo, A. P. Schnyder, and S. Ryu, “Classification of topological quantum matter with symmetries,” *Rev. Mod. Phys.* **88**, 035005 (2016).
- [23] I. Bloch, “Ultracold quantum gases in optical lattices,” *Nature Physics* **1**, 23–30 (2005).
- [24] D. P. Trauernicht, J. P. Wolfe, and A. Mysyrowicz, “Thermodynamics of strain-confined paraexcitons in Cu₂O,” *Phys. Rev. B* **34**, 2561–2575 (1986).
- [25] A. Klümper, A. Schadschneider, and J. Zittartz, “Matrix product ground states for one-dimensional spin-1 quantum antiferromagnets,” *EPL (Europhysics Letters)* **24**, 293 (1993).
- [26] A. M. Belemuk, N. M. Chtchelkatchev, A. V. Mikheyenkov, and K. I. Kugel, “Magnetic phase diagram and quantum phase transitions in a two-species boson model,” *Phys. Rev. B* **96**, 094435 (2017).
- [27] *See online Supplementary Information for more details.*
- [28] We considered only chains with even N , since the odd number is incompatible with antiferromagnetic order, resulting in slower numerical convergence.
- [29] D. P. Arovas, A. Auerbach, and F. D. M. Haldane, “Extended Heisenberg models of antiferromagnetism: Analogies to the fractional quantum Hall effect,” *Phys. Rev. Lett.* **60**, 531–534 (1988).
- [30] E. Bartel, A. Schadschneider, and J. Zittartz, “Excitations of anisotropic spin-1 chains with matrix product ground state,” *The European Physical Journal B - Condensed Matter* **31**, 209–216 (2003).
- [31] G. Vidal, “Efficient classical simulation of slightly entangled quantum computations,” *Phys. Rev. Lett.* **91**, 147902 (2003).
- [32] G. Vidal, “Efficient simulation of one-dimensional quantum many-body systems,” *Phys. Rev. Lett.* **93**, 040502 (2004).
- [33] G. Vidal, “Classical simulation of infinite-size quantum lattice systems in one spatial dimension,” *Phys. Rev. Lett.* **98**, 070201 (2007).
- [34] R. Orús, “A practical introduction to tensor networks: Matrix product states and projected entangled pair states,” *Annals of Physics* **349**, 117–158 (2014).
- [35] G. Vidal, J. I. Latorre, E. Rico, and A. Kitaev, “Entanglement in quantum critical phenomena,” *Phys. Rev. Lett.* **90**, 227902 (2003).
- [36] T. Kennedy and H. Tasaki, “Hidden symmetry breaking and the Haldane phase in $S=1$ quantum spin chains,” *Communications in Mathematical Physics* **147**, 431–484 (1992).
- [37] I. Affleck, T. Kennedy, E. H. Lieb, and H. Tasaki, “Valence bond ground states in isotropic quantum antiferromagnets,” *Comm. Math. Phys.* **115**, 477–528 (1988).
- [38] T. Kennedy and H. Tasaki, “Hidden $Z_2 \times Z_2$ symmetry breaking in Haldane-gap antiferromagnets,” *Phys. Rev. B* **45**, 304–307 (1992).
- [39] F. Haldane, “Continuum dynamics of the 1-D Heisenberg antiferromagnet: Identification with the $O(3)$ nonlinear sigma model,” *Physics Letters A* **93**, 464 – 468 (1983).
- [40] U. Schollwöck, J. Richter, D. J. Farnell, and R. F. Bishop, *Quantum magnetism*, Vol. 645 (Springer, 2008).
- [41] W. Chen, K. Hida, and B. C. Sanctuary, “Ground-state phase diagram of $S = 1$ XXZ chains with uniaxial single-ion-type anisotropy,” *Phys. Rev. B* **67**, 104401 (2003).

Supplementary Materials for “Topological spin phases of trapped Rydberg excitons in Cu₂O”

A.N. Poddubny and M.M. Glazov
Ioffe Institute, St. Petersburg 194021, Russia
(Dated: March 29, 2019)

CONTENTS

S1. Variational approximation for the ground state energy	1
S2. Dispersion of the excitations	2
S3. Role of the boundary conditions	3
S4. Ground state phase diagram	3
S5. Rydberg exciton states in a trap	4
References	5

S1. VARIATIONAL APPROXIMATION FOR THE GROUND STATE ENERGY

In this section we present the variational ansatz from Ref. [S1] that has allowed us to calculate the ground state energy in the infinite chain with the precision of better than 1%. This approach is based on the application of a nonlocal transformation (known as Kennedy-Tasaki transformation)

$$V = \prod_{j < k} \exp(i\pi S_j^z S_k^x) \quad (\text{S1})$$

to the Hamiltonian of the chain. The key advantage of the transformation Eq. (S1) is that it effectively “disentangles” the spins. This means that the ground state of the transformed Hamiltonian $\tilde{\mathcal{H}} = V\mathcal{H}V^{-1}$ can be sought in a simple factorizable form. Following Ref. [S1] it is sufficient to consider, after performing the transform in Eq. (S1) a chain with just two sites and the periodic boundary conditions, and look for the ground state in the form

$$\tilde{\psi}_{i_1 i_2} = \varphi_{i_1} \varphi_{i_2}, \quad (\text{S2})$$

where $i_1, i_2 = 1, 0, -1$ are the spin components and the “trial” spinor φ reads

$$\varphi = \frac{1}{\sqrt{u^2 + v^2 + 1}} \begin{pmatrix} u \\ 0 \\ v \end{pmatrix}. \quad (\text{S3})$$

The ground state energy is obtained by minimizing the expectation value of $\langle \tilde{\psi} | \tilde{\mathcal{H}} | \tilde{\psi} \rangle$ as a function of u and v . The dependence of this expectation value on the variational parameters is shown in Fig. S1. There exist four

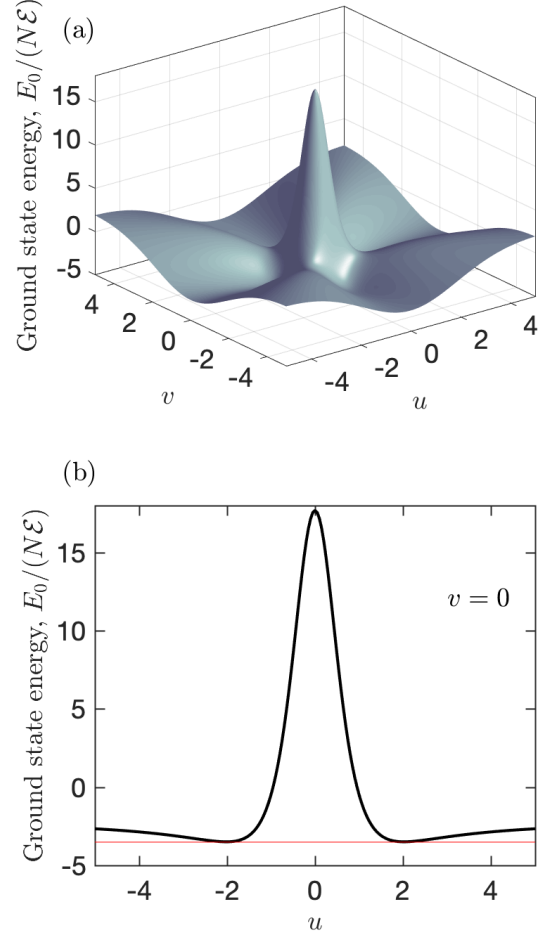


FIG. S1. Ground state energy depending on the variational parameters u and v in the state (S2), (S3). Panel (a) shows the dependence on both u and v demonstrating a maximum at $u = v = 0$ and four distinct minima, panel (b) shows the dependence on u at $v = 0$. Horizontal red line in the panel (b) indicates the numerically calculated ground state energy $E_0 = -3.51N\mathcal{E}$ in the infinite chain. The calculation has been performed for the same set of interaction constants as in the main text.

distinct minima for $u = \pm 2, v = 0, v = \pm 2, u = 0$. The presence of four minima for $u, v \neq 0$ can be interpreted as a spontaneous symmetry breaking effect. This so-called hidden $\mathbb{Z}_2 \times \mathbb{Z}_2$ symmetry is not obvious in the original Hamiltonian \mathcal{H} but is uncovered by the nonlocal Kennedy-Tasaki transformation. The minimum energy is $E_0 = -3.49N\mathcal{E}$, which is close to the exact value for the infinite chain $E_0 = -3.51N\mathcal{E}$ calculated by the

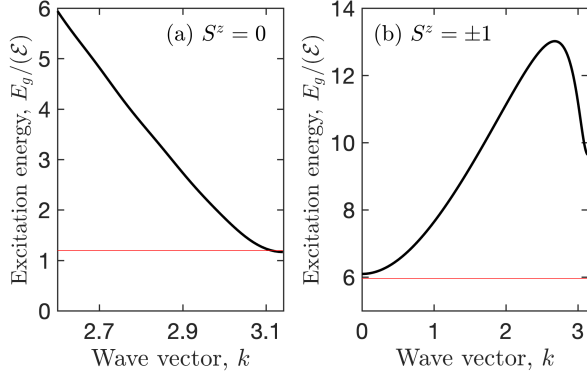


FIG. S2. Dispersion of the excitations with the total spin 0 (a) and the total spin 1 (b) in the infinite chain. Horizontal red lines show the excitation gap calculated numerically for a finite chain with $N = 14$ excitons $E_g = 1.19\mathcal{E}$ (a) and the gap to the $|S_z| = 1$ excitations $E_g = 5.96\mathcal{E}$ (b). The calculation has been performed in the single-magnon approximation.

iTEBD technique, cf. the black curve and the red line in Fig. S1(b).

Applying the operator Eq. (S1) to the state Eq. (S2) with $v = 0$, we obtain a ground state $V\tilde{\psi}$ in a matrix-product form

$$\psi_{i_1 i_2 i_3 \dots} \propto M_{\alpha_1 \alpha_2}^{i_1} M_{\alpha_2 \alpha_3}^{i_2} M_{\alpha_3 \alpha_4}^{i_3} \dots, \quad (\text{S4})$$

with

$$M^1 = \begin{pmatrix} 0 & 0 \\ -\frac{u}{\sqrt{u^2+1}} & 0 \end{pmatrix}, \quad M^{-1} = \begin{pmatrix} 0 & \frac{u}{\sqrt{u^2+1}} \\ 0 & 0 \end{pmatrix} \quad (\text{S5})$$

$$M^0 = \begin{pmatrix} -\frac{1}{\sqrt{u^2+1}} & 0 \\ 0 & \frac{1}{\sqrt{u^2+1}} \end{pmatrix},$$

where the indices $i_j = 0, +1, -1$ label the projections of the spin j . The rank-two matrices M describe the correlations and entanglement between the spins. Thus, as expected from general analysis, the variational approach of Ref. [S1] gives a simplified version of the matrix-product wavefunction.

S2. DISPERSION OF THE EXCITATIONS

Here we present the variational calculation of the dispersion $E_g(k)$ of the lowest excitations in the infinite exciton chain.

It has been proved that the spectrally separated excitations of a non-critical translation-invariant system can be arbitrarily well approximated by building a momentum superposition of a local operator acting on the ground state [S2]. For our purposes it is sufficient to use the most simple single-magnon approximation [S3, S4]. The excitation with the total spin equal to zero is sought in

the following form

$$\psi_k \propto \frac{1}{\sqrt{N}} \sum_{j=1}^N e^{ikj} S_j^z |0\rangle, \quad (\text{S6})$$

where $|0\rangle$ is the numerically calculated ground state. The excitation energy is then given by

$$E_g(k) = \frac{s(k)}{2f(k)} \quad (\text{S7})$$

where

$$s(k) = \frac{1}{N} \sum_{jj'} e^{ik(j-j')} \langle 0 | [S_{j'}^z, [H, S_j^z]] | 0 \rangle \quad (\text{S8})$$

and

$$f(k) \equiv \langle 0 | S_{-k}^z S_k^z | 0 \rangle = \frac{1}{N} \sum_{jj'} e^{ik(j-j')} \langle 0 | S_{j'}^z S_j^z | 0 \rangle \quad (\text{S9})$$

is the structure factor. The main advantage of the single-magnon approximation is that it directly expresses the excitation energy via the spin-spin correlations in the ground state. Hence, once the ground state is obtained by the iTEBD technique, the dispersion of excitations can be calculated without significant additional numerical cost. The precision can be further improved by expanding the set of the variational functions [S5, S6]. The results of variational calculations in the $S_z = 0$ sector of excitations are shown in Fig. S2(a) in the vicinity of $k = \pi$, where the minimum of the dispersion is realized.

In the case of spin-1 excitation, the variational function should be described by the two parameters [S4]

$$\psi_k \propto \frac{1}{\sqrt{N}} \sum_{j=1}^N e^{ikj} [\mu_1 S_j^z + \mu_2 S_j^z (S_j^x \pm i S_j^y)] \psi_0, \quad (\text{S10})$$

The excitation energy is then found from a generalized 2×2 eigenproblem

$$\mathcal{H}(k)\psi = E_g(k)\mathcal{W}\psi, \quad (\text{S11})$$

where

$$\mathcal{H}_{\alpha\beta}(k) = \sum_{jj'} e^{ik(j-j')} \langle 0 | O_j^\alpha H O_j^\beta | 0 \rangle, \quad (\text{S12})$$

$$\mathcal{W}_{\alpha\beta}(k) = \sum_{jj'} e^{ik(j-j')} \langle 0 | O_j^\alpha O_j^\beta | 0 \rangle \quad (\text{S13})$$

and $O_j^1 = S_j^z$, $O_j^2 = S_j^z (S_j^x + i S_j^y)$. The results of the calculation are presented in Fig. S2(b). Here the minimum is realized in the vicinity of the $k = 0$ point. The variational results for the excitation gaps are in agreement with the rigorous numerical calculation for small finite chains shown in Fig. 2 of the main text, see also horizontal red lines in Fig. S2.



FIG. S3. Structure of the ground eigenstate in the AKLT model with $\mathcal{H}_{\text{bond}} = \mathbf{S}_1 \cdot \mathbf{S}_2 + (\mathbf{S}_1 \cdot \mathbf{S}_2)^2/3$ [S1, S7]. Each spin 1 (oval) is represented by triplet states of two spins 1/2 (dots). The spins 1/2 for neighboring sites are bound into singlets (blue lines). Two dangling spins remain in the finite chain (yellow dots) explaining the 4-fold degeneracy of the ground state in long chain with open ends.

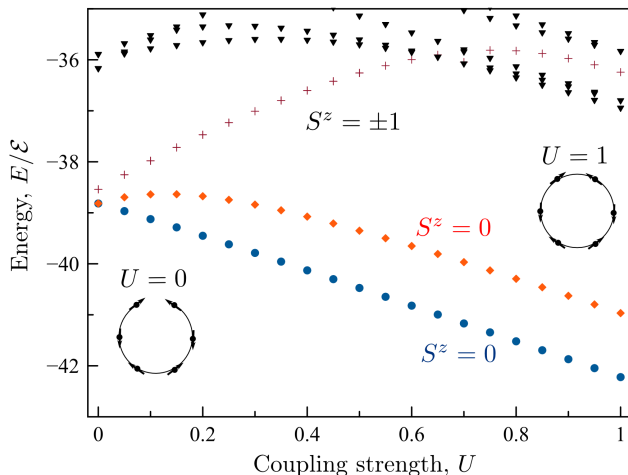


FIG. S4. Energies of the several lowest states in the exciton chain depending on the coupling parameter U in Eq. (S14), controlling the boundary conditions. The insets schematically illustrate the limiting cases of an open chain ($U = 0$) and a ring ($U = 1$). Calculation has been performed for $N = 12$ excitons.

S3. ROLE OF THE BOUNDARY CONDITIONS

The distinctive topological feature of the Haldane phase is the strong sensitivity of the ground state to the choice of boundary conditions, either open ones or periodic ones [S7]. This effect can be understood in the simplest fashion for the isotropic Affleck-Kennedy-Lieb-Tasaki (AKLT) model with $\mathcal{H}_{\text{bond}} = \mathbf{S}_1 \cdot \mathbf{S}_2 + (\mathbf{S}_1 \cdot \mathbf{S}_2)^2/3$. Each of the spins 1 (oval) can be equivalently replaced by three-fold degenerate triplet states of *two* strongly interacting spins 1/2 (circles). Next, the interaction between the sites leads to coupling of neighboring spins 1/2 (otherwise degenerate) into a singlet states. Two dangling spins (yellow dots) remain on the opposite edges of the finite chain, hence, the ground state becomes fourfold degenerate in the infinite chain limit, see Fig. S3. When the open chain is closed and transformed to a ring, the dangling edge spins are fused together and the ground state becomes non-degenerate. Similar effect is expected for the Haldane phase realized in our case of strongly anisotropic chain of Rydberg excitons.

In order to examine these dramatic boundary effects in our system, we have explicitly analyzed the transition

between an open chain and a closed ring, both described by a Hamiltonian

$$\mathcal{H} = \sum_{j=1}^{N-1} \mathcal{H}_{\text{bond}}(\mathbf{S}_j, \mathbf{S}_{j+1}) + U \mathcal{H}_{\text{bond}}(\mathbf{S}_N, \mathbf{S}_1). \quad (\text{S14})$$

Here, the parameter U controls the boundary conditions: the value of $U = 1$ corresponds to the periodic boundary conditions, i.e. spins on a ring. When $U = 0$, the ring is broken and the boundary conditions correspond to an open chain. Figure S4 presents the energy spectrum calculated by full diagonalization for a small chain with $N = 12$ excitons. It demonstrates that the ground state of the open chain has almost exact 4-fold degeneracy. The four bottom levels can be understood as the combinations of edge spins-1/2. Namely, four spins 1/2 can form a singlet with a zero total spin and a triplet with the total spin S equal to one. The triplet states with $S^z = \pm 1$ are degenerate due to the time inversion symmetry. The two states with $S^z = 0$, stemming from a singlet and a triplet, are slightly split due to the finite size of the chain. When the coupling parameter U is increased, the ground state is dramatically modified and transforms from an (almost) four-fold degenerate one to a non-degenerate one, reflecting the fusion of the edge 1/2 spins. The energy of one of the states with $S^z = 0$ decreases by $\approx E_0 = -3.5E$, since an extra bond is formed in a system. The second state with $S^z = 0$, being degenerate with the ground state in the open chain, becomes in a first excited state of the close ring, corresponding to a magnon mode from Fig. S2(a). The states with $S^z = 1$ increase in energy and are also transformed to the magnon modes from Fig. S2(b). Importantly, the comparison of the limits $U = 0$ (open chain) and $U = 1$ (ring) shows that the degeneracy of the ground state is higher for the open chain being an evidence of edge uncoupled spins appearing in the system.

S4. GROUND STATE PHASE DIAGRAM

In this section we present the numerical data behind the phase diagram of the ground state, Fig. 4 in the main text. In order to obtain the phase diagram we have calculated the spin-spin and string correlators in the ground state at large odd and even distances ($j = 39$ and $j = 38$, respectively) which exceed by far the correlation lengths in our system ($N_0 \sim 7$, Fig. 3 of the main text). The results are presented in Fig. S5. The Haldane phase corresponds to the vanishing spin-spin and nonzero string correlations, white circle in Fig. S5. On the other hand, in the ferromagnetic and antiferromagnetic phases both string correlations and spin-spin correlations are nonzero. The phases can be distinguished by the relative sign of the correlations for j and $j+1$, positive for the ferromagnetic phase and negative for the antiferromagnetic phase. The disordered phase does not display correlations.

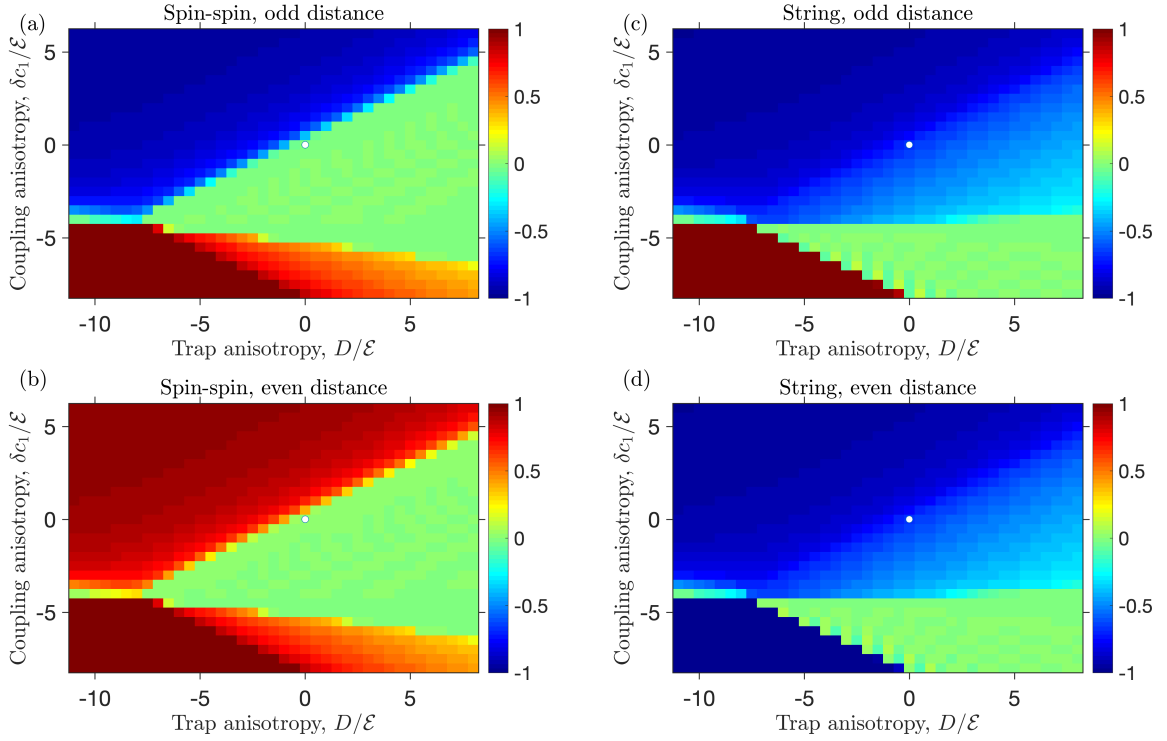


FIG. S5. Spin-spin correlators $\langle S_0^z S_j^z \rangle$ (a,c) and string correlators $\langle S_0^z e^{i\pi(S_1^z + S_2^z + \dots + S_{j-1}^z)} S_j^z \rangle$. Panels (a,b) and (c,d) correspond to odd and even spin-spin distances, $j = 39$ and $j = 38$, respectively. White circle indicates the parameters of Ref. S8 ($D = \delta c_1 = 0$).

S5. RYDBERG EXCITON STATES IN A TRAP

The single particle states of the Rydberg exciton in a trap are described by the Hamiltonian

$$\mathcal{H}_x = -\frac{\hbar^2}{2\mu}\Delta_\rho - \frac{e^2}{\varkappa\rho} - \frac{\hbar^2}{2M}\Delta_{\mathbf{R}} + V(\boldsymbol{\rho}, \mathbf{R}), \quad (\text{S15})$$

acting on the wavefunction of the electron-hole pair, $\Psi(\boldsymbol{\rho}, \mathbf{R})$. Here we use the center-of-mass, $\mathbf{R} = (m_e \mathbf{r}_e + m_h \mathbf{r}_h)/M$, and relative motion, $\boldsymbol{\rho} = \mathbf{r}_e - \mathbf{r}_h$, coordinates, μ and M are the reduced and translational masses of the electron-hole pair, respectively, m_e and m_h are the masses of the electron and the hole, and \mathbf{r}_e and \mathbf{r}_h are their coordinates, \varkappa is the dielectric constant. In Eq. (S15) $V(\boldsymbol{\rho}, \mathbf{R}) = V_e(\mathbf{r}_e) + V_h(\mathbf{r}_h)$ is the confinement potential being the sum of the electron and hole potential energies in the trap.

In the absence of the trap the exciton wavefunction is decomposed as a product of the center of mass and relative motion wavefunctions, $\Psi(\boldsymbol{\rho}, \mathbf{R}) = \psi(\mathbf{R})\Phi(\boldsymbol{\rho})$. The states of the relative motion

$$\Phi_{n,l,m}(\boldsymbol{\rho}) = R_{nl}(\rho)Y_{lm}(\vartheta, \varphi), \quad (\text{S16})$$

form hydrogen-like series with $n = 1, 2, \dots$ being the principal quantum number, $l = 0, 1, \dots, n$ being the orbital angular momentum and $m = -l, \dots, l$ being its component or magnetic quantum number [S9, S10]; $\rho = |\boldsymbol{\rho}|$, ϑ

and φ are the angles of the $\boldsymbol{\rho}$. The effects related to the crystalline anisotropy are disregarded [S11, S12].

We take the trap potential in the simplest possible form assuming that electron and hole are confined by the parabolic potential. The presence of the trap does not allow one, in general, to separate the electron and hole coordinates, however, for particular choice of the trap parameters (where the oscillator frequencies for both carriers are the same [S13, S14]) the trap potential can be recast as

$$V(\boldsymbol{\rho}, \mathbf{R}) = \frac{\mu\Omega_\perp^2}{2}(x^2 + y^2) + \frac{\mu\Omega_\parallel^2}{2}z^2 + \frac{M\Omega_\perp^2}{2}(X^2 + Y^2) + \frac{M\Omega_\parallel^2}{2}Z^2. \quad (\text{S17})$$

Here z is the trap axis, x , y and z are the Cartesian components of the relative motion position-vector, $\boldsymbol{\rho}$, and X , Y and Z are the Cartesian components of the center of mass motion position-vector \mathbf{R} , Ω_\parallel and Ω_\perp are the corresponding frequencies for the confinement along the trap axis and perpendicular to the trap axis, respectively. The center of mass quantization is described by the series of harmonic oscillator states with equidistant levels.

For $\Omega_\parallel = \Omega_\perp$ the relative motion states can be still represented in the form of Eq. (S16) due to spherical symmetry of the problem. In this case three p -shell states, p_x , p_y and p_z corresponding to the linear combinations of $l = 1$, $m = \pm 1$ and 0 states are equivalent and have

the same energies. By contrast, for $\Omega_{\parallel} \neq \Omega_{\perp}$ the splitting between the doublet p_x, p_y and the singlet p_z state appears. For the prolate trap, $\Omega_{\parallel} < \Omega_{\perp}$, the p_z state has a lower energy, while for the oblate trap, $\Omega_{\parallel} > \Omega_{\perp}$, the p_z state energy increases. The effective orbital angular momentum dependent Hamiltonian reads

$$\mathcal{H}_1 = D \left(S_z^2 - \frac{2}{3} \right), \quad (\text{S18})$$

where we excluded the overall energy shift of the $l = 1$ triplet. The parameter D is proportional to $\Omega_{\parallel} - \Omega_{\perp}$.

To quantify the scenario we assume that the trap po-

tential is weak and can be treated by means of the first-order perturbation theory. Making use of the radial integrals we obtain

$$\int R_{nl=1}^2(\rho) \rho^4 d\rho = \frac{5}{2} n^2 (n^2 - 1) \left(\frac{\hbar^2 \varkappa}{\mu e^2} \right)^2,$$

we obtain for the parameter D in Eq. (S18)

$$D = \frac{\mu(\Omega_{\parallel}^2 - \Omega_{\perp}^2)}{2} \left(\frac{\hbar^2 \varkappa}{\mu e^2} \right)^2 n^2 (n^2 - 1). \quad (\text{S19})$$

-
- [S1] T. Kennedy and H. Tasaki, “Hidden $Z_2 \times Z_2$ symmetry breaking in Haldane-gap antiferromagnets,” *Phys. Rev. B* **45**, 304–307 (1992).
- [S2] J. Haegeman, S. Michalakis, B. Nachtergaele, T. J. Osborne, N. Schuch, and F. Verstraete, “Elementary excitations in gapped quantum spin systems,” *Phys. Rev. Lett.* **111**, 080401 (2013).
- [S3] D. P. Arovas, A. Auerbach, and F. D. M. Haldane, “Extended Heisenberg models of antiferromagnetism: Analogies to the fractional quantum Hall effect,” *Phys. Rev. Lett.* **60**, 531–534 (1988).
- [S4] E. Bartel, A. Schadschneider, and J. Zittartz, “Excitations of anisotropic spin-1 chains with matrix product ground state,” *The European Physical Journal B - Condensed Matter* **31**, 209–216 (2003).
- [S5] J. Haegeman, T. J. Osborne, and F. Verstraete, “Post-matrix product state methods: To tangent space and beyond,” *Phys. Rev. B* **88**, 075133 (2013).
- [S6] V. Zauner, D. Draxler, L. Vanderstraeten, M. Degroote, J. Haegeman, M. M. Rams, V. Stojevic, N. Schuch, and F. Verstraete, “Transfer matrices and excitations with matrix product states,” *New Journal of Physics* **17**, 053002 (2015).
- [S7] I. Affleck, T. Kennedy, E. H. Lieb, and H. Tasaki, “Valence bond ground states in isotropic quantum antiferromagnets,” *Comm. Math. Phys.* **115**, 477–528 (1988).
- [S8] V. Walther, S. O. Krüger, S. Scheel, and T. Pohl, “Interactions between Rydberg excitons in Cu_2O ,” *Phys. Rev. B* **98**, 165201 (2018).
- [S9] L. Landau and E. Lifshitz, *Quantum Mechanics: Non-Relativistic Theory* (Butterworth-Heinemann, Oxford, 1977).
- [S10] T. Kazimierczuk, D. Fröhlich, S. Scheel, H. Stolz, and M. Bayer, “Giant Rydberg excitons in the copper oxide Cu_2O ,” *Nature* **514**, 343 (2014).
- [S11] J. Thewes, J. Heckötter, T. Kazimierczuk, M. Aßmann, D. Fröhlich, M. Bayer, M. A. Semina, and M. M. Glazov, “Observation of high angular momentum excitons in cuprous oxide,” *Phys. Rev. Lett.* **115**, 027402 (2015).
- [S12] F. Schweiner, J. Main, M. Feldmaier, G. Wunner, and C. Uihlein, “Impact of the valence band structure of Cu_2O on excitonic spectra,” *Phys. Rev. B* **93**, 195203 (2016).
- [S13] W. Que, “Excitons in quantum dots with parabolic confinement,” *Phys. Rev. B* **45**, 11036 (1992).
- [S14] M. A. Semina, R. A. Sergeev, and R. A. Suris, “Localization of electron-hole complexes at fluctuations of interfaces of quantum dots,” *Semiconductors* **40**, 1338–1345 (2006).